# *Ab initio* studies of hydrogen adatoms on bilayer graphene

R. E. Mapasha,[1] A. M. Ukpong,[1,*] and N. Chetty[1,2]

[1]*Department of Physics, University of Pretoria, Pretoria 0002, South Africa*
[2]*National Institute for Theoretical Physics, Johannesburg, 2000, South Africa*

(Dated: April 23, 2012)

We present a comparative density functional study of the adsorption of hydrogen on bilayer graphene. Six different exchange-correlation functionals are employed to explore the possible configurations of hydrogen adsorption at 50% coverage. Using the four variants of the non-local van der Waals density functional, we identify three distinct competing configurations that retain the coupled bilayer structure at 0 K. One of the configurations undergoes a spontaneous transformation from hexagonal to tetrahedral structure, under hydrogenation, with heat of formation ranging between -0.03 eV (vdW-DF) and -0.37 eV (vdW-DFC09$_x$). This configuration has a finite band gap of around 3 eV, whereas all other competing configurations are either semi-metallic or metallic. We also find two unique low-energy competing configurations of decoupled bilayer graphene, and therefore suggest the possibility of graphene exfoliation by hydrogen intercalation.

PACS numbers: 71.15.Nc, 71.20.-b, 73.20.Hb, 73.22.Pr

## I. INTRODUCTION

Graphene, a free-standing single-atom thick layer of graphite, was first isolated in 2004.[1] The first production of graphene involved the ex-foliation and cleavage methods. These involve the peeling of single-atom thick layers from bulk highly-oriented pyrolytic graphite (HOPG).[1] Graphene has remarkable properties, such as the anomalous quantum Hall effect, high carrier mobility and ballistic transport up to room temperatures.[2–6] These properties suggest that graphene can be a reliable candidate for applications in nanotechnology and microelectronic devices.[7] The local network structure of graphene, just as in graphite, consists of sp$^2$-hybridized carbon bonds. In the plane of the hexagonal lattice, each carbon atom is bonded to three nearest neighbors by strong $\sigma$-bonds.[8] In addition, there is a weak $\pi$-bond localized on each carbon atom. The resulting band structure shows the $\pi$-bands near the Fermi level.[3,8] These arise from orbitals located near the $K$ and $K'$ points on opposite corners of the Brillouin zone. The electronic signatures of the $\pi$-bands are uniquely characterized by a Dirac-like dispersion at the $\Gamma$-point. These form linear dispersions, at the $K$-point. Since the valence and conduction bands meet at the $K$-point, graphene exhibits a zero band gap.[3,8] The resulting semi-metallic behavior therefore limits the range of applicability of graphene monolayers in nanotechnological and microelectronic applications.

As a result, concerted efforts have been directed towards tuning the band gap in graphene monolayers both experimentally[9–15] and theoretically.[16–24] There are various ways in which the graphene structure has been explored. These include producing nanoribbons,[25–27] rotating the carbon atoms at specific angles to form Stone-Wales-type defects,[18,21,28–32] and adsorbing different impurities on the monolayer.[9–24] The latter has been regarded as the most promising method because the adsorption of hydrogen modifies the local structure significantly. At 100 % hydrogen-coverage, the local structure is completely transformed from sp$^2$ to sp$^3$ hybridized carbon bonds.[14,15,24] Adsorption of hydrogen atoms on graphene was first studied experimentally by Elias *et al.*[15] and theoretically by Sofo *et al.*[24] The band gap was found to be 3.5 eV in both cases. However, more recent studies[16–23] have focused on the energetics, and structural stability of the graphene monolayer using density functional theory (DFT).

Bilayer graphene is a stacked double layer of graphene, which is weakly bound by van der Waals forces. It possesses interesting electronic properties, which are slightly different from those of single layer graphene. In bilayer graphene, electrons behave as massive chiral fermions,[33,34] whereas they behave as massless Dirac fermions in single layer graphene.[6] This results in ballistic electron transport seen in the graphene monolayer. The linear dispersion around the $K$-point in a graphene monolayer becomes parabolic in bilayer graphene.[33] However, the valence and conduction bands also meet at the $K$-point of the Brillouin zone. This arrangement of bands indicate that bilayer graphene is also semi-metallic.[33,34] Experimentally, the first attempt to open the band gap in bilayer graphene was successfully achieved by the application of a strong electric field perpendicular to the graphene planes.[35] In addition, this has been achieved by chemical modification of the local structure,[15,19,22,34,36–39] and by the application of uniaxial strain on the structure.[40,41] Just as in single layer graphene, the hydrogen adatoms were considered to be the preferred candidates to facilitate the transformation of the structure from a semimetal to an insulator.

Luo *et al.*[36] reported that the hydrogenation of a few single layers of graphene is less feasible than those of bilayer and trilayer graphene. They also showed experimentally that the hydrogenation and dehydrogenation of graphene depends on the number of monolayers. They found that, depending on the plasma power, the hydrogen coverage can be manipulated up to the saturation level of 100 % H-coverage. Furthermore, Subrahmanyam *et al.*[37] demonstrated the possible use of few layer graphene in hydrogen storage. They showed that few layer graphene can contain up to 5 wt% of hydrogen, which is more than the 3 wt% stored in carbon nanotubes. Their spectroscopic measurements on hydrogenated bilayer graphene showed that the local structure contains some sp$^3$-hybridized carbon bonds. They also observed that hydrogen decomposes when the structure is heated up to 500 °C. Jaiswal *et al.*[38]

investigated the electronic properties of graphene sheets at different degrees of hydrogenation using Raman and charge transport spectroscopies. They showed that partially hydrogenated mono- and bi-layer graphene has weak insulating behavior, and that bilayer graphene is more readily affected by hydrogen compared to few single layers of graphene, in agreement with the measurements of Luo *et al.*[36]

Few single layers of graphene (SLG) contain more than three bound graphene monolayers. The observation by Elias *et al.*,[15] that the SLG is far more receptive to hydrogen than bilayer graphene is in direct contrast to the measurements of Luo *et al.*[36] Earlier, Boukhvalov *et al.*[19] performed a comparative study of hydrogen adsorption on single and bilayer graphene using DFT. They considered the single hydrogen and pair of hydrogen adatoms and found that the lattice distortions were different in single and bilayer structures. They observed that the distance between any two bonded carbon atoms in the bilayer is less than the equivalent distance in the single layer. This is because the interlayer interaction makes the layers to remain flat. Based on the chemisorption energies, they concluded that in both structures, the pair of hydrogen adatoms stabilizes the structure better than the single hydrogen adatom.[19] This conclusion was also validated using the activation energies, since the single and pair of hydrogen adatoms yielded positive and negative activation energies, respectively. They also found that the hydrogenated monolayer is far more stable than the hydrogenated bilayer graphene. Later on, Boukhvalov *et al.*[22] argued that the maximum hydrogen coverage on bilayer graphene is 25 %, and that this configuration gives the most stable structure. At 25 % coverage, the interlayer distance reduces to 3.25 Å from the 3.35 Å obtained in pristine bilayer graphene. In this configuration, the band structure showed a wide gap between the conduction and valence bands.

Leenaerts *et al.*[39] investigated the possibility of 50 % hydrogen coverage on bilayer graphene. The interlayer distance was found to reduce significantly, resulting in the creation of strong covalent bonds that stabilize the structure. However this transformation only occurs when the hydrogen is adsorbed on top of an indirect carbon atom (*i.e,* on top of the carbon atom that faces the center of the hexagon on the opposite layer). In this configuration, the unhydrogenated carbon atom faces another unhydrogenated carbon atom on the opposite layer. The resulting structure has a wide band gap. Nevertheless, the formation energy is still higher than that of the hydrogenated single layer graphene. On this basis, they also concluded that the hydrogenated single layer is more stable than the hydrogenated bilayer graphene.

Previous DFT investigations of hydrogen adsorption on graphene mono-, bi-, and few single layers of graphene have so far, not included the effects of van der Waals interactions. Besides, Boukhvalov *et al.*[19] investigated the chemisorption of a single H atom, and a pair of H atoms on a 32-atom supercell. These two configurations correspond to hydrogen coverage of 3.1% and 6.3%, respectively. In particular, these two levels of hydrogen coverage are low, and insufficient to capture the H-induced transformations of the bilayer graphene structure. Moreover, the more recent investigation of Leenaerts *et al.*[39] considered a single configuration for hydrogen adsorption at 50% coverage. Because previous studies only focused on hydrogenating the top and bottom external faces of the graphene bilayer,[39] we consider also the hydrogenation of the interlayer faces.

We present a comparative density functional study of the structural configurations of hydrogen adsorption on bilayer graphene. In our work, the number of hydrogen adatoms is always chosen to be 50 % coverage in each of the configurations. Leenaerts *et al.*[39] suggested this as the maximum possible H-coverage on bilayer graphene. This has motivated us to systematically investigate the stable competing low-energy configurations that may exist at this level of hydrogenation. The aim is to identify energetically favorable configurations and identify competing low energy structures at 0 K. We also investigate the influence of H-adatoms on the electronic properties of bilayer graphene within the framework of density functional theory, using different exchange-correlation (XC) potentials. We show that no single XC functional is able to reproduce all the known physical properties of all the configurations considered. The relative strengths and weaknesses of the functionals are discussed.

## II. METHODOLOGY

The ground state electronic structure was calculated using the plane wave self-consistent field (PWSCF) code as implemented in the Quantum ESPRESSO package.[42] The calculations were first performed using the local density and the generalized gradient approximations (LDA)[43] and (GGA)[44] for the exchange-correlation interaction. We used the GGA parameterization of Perdew, Burke and Ernzerhof (PBE).[44] Thereafter, the Roman-Perez and Soler implementation[45] of the non-local van der Waals density functional (vdW-DF) theory of Dion *et al.*[46] was used to study the ground state properties of graphite, pristine and hydrogenated bilayer graphene. The second version of the van der Waals density functional (vdW-DF2) theory proposed by Lee *et al.*[47] was also used to calculate the properties of these materials for comparison. In the vdW-DF2 calculations, an accurate refit[48] of the Perdew-Wang (PW86) semilocal exchange functional[49] was used. Furthermore, the exchange functional ($C09_x$) of Cooper[50] was also used within the two vdW-DF schemes to perform a comparative study of these materials, and results from these two schemes are denoted as vdW-DF$C09_x$ and vdW-DF2$C09_x$.

The core electron interactions were described using the projector augmented wave (PAW) methods.[51] Energy cut-offs of 500 and 5170 eV were set for the wave function and charge density expansions, respectively, in the plane waves basis. The Monkhorst-Pack scheme[52] was used for the integration of electronic states, using a grid of size $10 \times 10 \times 1$. The Methfessel-Paxton (MP) scheme[53] was used in the self-consistent field calculations, with a smearing width of 0.3 eV. The total energies were converged to within $10^{-7}$ eV. The supercells were optimized using the conjugate gradient algorithm with an atomic force convergence criterion of 0.01 eV/Å. In each case, the graphite and bilayer graphene struc-

tures were modeled using a $1 \times 1$ periodic unit cell. The vacuum height was set to 15 Å to avoid spurious interactions between periodically repeated images of the graphene bilayer system.

## III. RESULTS AND DISCUSSION

### A. Test of exchange-correlation functionals on bulk bilayer graphene and graphite

In this section, the different exchange-correlation functionals are tested on the properties of graphite and bilayer graphene. In bilayer graphene, the two monolayers are arranged in two distinct stacking sequences - the simple (AA) and Bernal (AB) conformations. Results show that the Bernal stacking gives a more stable bilayer graphene structure than the simple stacking sequence. The AB-stacked structure gives a total energy per atom, which is 0.02 eV (LDA), 0.01 eV (GGA) and 0.01 eV (vdW-DF) lower than the corresponding total energy in the simple stacking sequence. The LDA total energy difference is consistent with the results of De Andres *et al.*[41] In addition, the AB-stacking sequence consistently yields stronger interlayer binding from all the XC functionals. For instance, the simple stacking sequence gives an interlayer separation that is 0.21 Å (LDA), 0.02 Å (GGA) and 0.22 Å (vdW-DF) larger than the corresponding distance in a Bernal stacked structure. As a result, we will not discuss the AA-stacked bilayer graphene any further and all subsequent adsorption studies are reported for the AB-stacked structures.

Table I shows the lattice constant ($a_0$), interlayer distance ($d_0$), and the interlayer binding energy($E_B$) of graphite and pristine bilayer graphene from different form of exchange correlation functionals. The interlayer binding energy in this case, is the total energy difference between the two coupled and uncoupled graphene layers. The properties of the bilayer, *i. e.* lattice constant and interlayer distance, are generally similar to those of graphite as expected. For instance, although slightly smaller than the experimental value (2.46 Å) in both structures,[58] the optimized LDA lattice constant (2.45 Å) is the same for bilayer graphene and graphite. The difference between their corresponding GGA values is less than 1%. This trend is also consistent with other LDA and GGA calculations.[54] The LDA interlayer distance is 3.25 Å for graphite and 3.33 Å for bilayer graphene. In both structures, the GGA predicts the same value (4.10 Å) for $d_0$ but overestimates the experimental value substantially (see Table I). More significant differences are observed between our GGA-PBE values, and the GGA-PBE(DCAP) data[62] for $d_0$ and $E_B$ respectively. Nevertheless, there is good agreement between our results and similar calculations. The calculated LDA interlayer binding energy of graphite is 27.70 meV/atom. Our calculated LDA bilayer binding energy decreases to 17.30 meV/atom. This value is nearly half the experimental value of the binding energy in graphite. As expected, results of our GGA calculations fail to accurately describe structures that are bounded together by van der Waals forces (see Table I). We also tested the structural properties of the bilayer and graphite using different variants of the van der Waals (vdW) corrections to DFT. Our calculated vdW-DF lattice constants for graphite and bilayer graphene are 2.48 Å and 2.47 Å respectively, in good agreement with results of other vdW-DF calculations.[55,56]

Our vdW-DF optimized interlayer distance of 3.50 Å is intermediate between the GGA and LDA values for both graphite and bilayer graphene. However, this is closer to the LDA value than to the GGA value. On the other hand, vdW-DF2 yields the same structural properties for graphite and the bilayer. For graphite, we find that using the Cooper exchange functional ($C09_x$) within the vdW scheme results in the highest interlayer binding energy of 91.00 meV (vdW-DFC09$_x$). This value is 18.00 meV higher than the exfoliation energy predicted for graphite within the vdW-DFC09$_x$ scheme.[54] However, within the vdW-DF2C09$_x$ scheme, the interlayer binding energy reduces to 59.60 meV. Consider that the graphite interlayer binding energies of 55.00 meV (vdW-DF) and 66.00 meV (vdW-DF2) are significantly lower, prior to correction with $C09_x$ functional. Because the structural properties of graphite predicted within the vdW-DFC09$_x$ scheme, in Table I, agree with experimental values to within ±3%, we attribute the large discrepancy in interlayer binding energy to the inability of the vdW-DFC09$_x$ functional to simultaneously describe the energetics and the structural properties consistently. In Ref. 57 however, bilayer graphene is used as a model to estimate the binding energy of graphite as 45.50 meV/atom using the vdW-DF scheme. It is therefore expected, *a posteri*, that bilayer graphene should have nearly the same binding energy. The calculated bilayer binding energy is 22.70 meV/atom (vdW-DF) and 29.00 meV/atom (vdW-DF2), which are 50% and 36% smaller than anticipated. Nevertheless, our vdW-DF and vdW-DF2 values are within the range of the results of other similar calculations (see Table I).

The use of the Cooper exchange functional ($C09_x$) shows a substantial increase to 38.90 eV/atom (vdW-DFC09$_x$), and a marginal increase to 28.60 meV/atom (vdW-DF2C09$_x$) in each case. Taken together, the vdW-interaction corrections give bilayer binding energy that agree with the experimental value of 35±10 meV/atom for graphite, in agreement with previous vdW-DF calculations.[54] However, more recent experiments show a substantially higher interlayer binding energy of 52±50 meV/atom in graphite.[59] This is significantly higher than the calculated bilayer binding energy, but consistent with our calculated values for graphite. We attribute this discrepancy to the inability of the functionals to simultaneously account for both the structural properties and the binding energies of weakly bound structures that are coupled together by vdW forces.

### B. Hydrogen adatoms on bilayer graphene

#### 1. *Site geometries for hydrogen adsorption*

The unrelaxed site geometries for hydrogen adsorption on the bilayer graphene unit cell are shown in Fig. 1. Because H prefers the on-top site,[39] each coupled bilayer graphene con-

figuration has the H atoms occupying on top sites in the unrelaxed state. However, we do not consider the case of hydrogen adsorption at both the on top and bottom sites of the same carbon atom - even if such configurations can, in principle, give 50 % H coverage in the unrelaxed state. This is to preserve the hexagonal symmetry of the $sp^2$-hybridized carbon bonding in bilayer graphene prior to relaxation. In the following analysis, the carbon atoms that directly face another carbon atom (i.e., a and b′ in Fig. 1) are labeled direct carbon atoms, whereas indirect carbon atoms face hollow sites in the adjacent layer (i.e., b and a′ in Fig. 1). In all the unrelaxed configurations, the interlayer distance is the same, and the C-C distance is unique in both A- and B-planes, by symmetry.

A total of 24 non-unique configurations are identified for cases where the two hydrogen atoms are adsorbed at on top sites on two different carbon atoms. From translational symmetry, this reduces to 18 configurations. In Fig. 1, planes A and B are invariant under 180 ° rotation. After correcting for double counting, only the 16 configurations listed in Table II are unique in the unrelaxed state. We find that some configurations are energetically equivalent after relaxation in spite of the uniqueness of their initial unrelaxed states.

For instance, three distinct cases are identified for formation of molecular hydrogen after relaxation. The dimer forms above the coupled bilayer structure in configuration $c_1$ as shown in Fig. 2(a), and within the interlayer region in configurations $c_{12}$, $c_{14}$ and $c_{15}$. Because the dimer is oriented horizontally in both configurations $c_{12}$ and $c_{14}$ (see Fig. 2(b)), we conclude that both configurations are energetically equivalent. On the other hand, the dimer in configuration $c_{15}$ is oriented vertically (Fig. 2(c)), and therefore represents a unique configuration, and distinct from configuration $c_{12}$ or $c_{14}$. The three cases of dimer formation are energetically non-equivalent and unique, suggesting that their unrelaxed states are not stable. As a result, we investigate the physisorption of the $H_2$ dimer above bilayer graphene, and within the interlayer region as special cases of the hydrogen adsorption.

Each of the four schemes for correcting for vdW-interaction predict the same interlayer distances for the two configurations of the horizontally-oriented dimer as: 6.67 Å (vdW-DF), 6.29 Å (vdW-DF2), 6.19 Å (vdW-DFC09$_x$) and 6.14 Å (vdW-DF2C09$_x$) respectively. In configuration $c_{15}$ the dimer is vertically oriented, and the interlayer distance changes slightly to 6.93 Å (vdW-DF), 6.53 Å (vdW-DF2), 6.26 Å (vdW-DFC09$_x$) and 6.22 Å (vdW-DF2C09$_x$) respectively. When the Cooper (C09$_x$) functional is used within the two vdW-DF schemes, the interlayer distances only reduce slightly. Because of this marginal reduction in interlayer distance, we conclude that vdW-DFC09$_x$ and vdW-DF2C09$_x$ schemes both predict slightly stronger binding in the two cases of interlayer dimer formation. Nevertheless, the trend for variation in interlayer distances with exchange-correlation functional in configuration $c_{12}$, $c_{14}$ and $c_{15}$ is not uniform. For instance, although all the functionals consistently yield large values of $d_0$, the variations in $d_0$ with vdW-DF correction scheme are non-uniform. Particularly, the vdW-DF2, vdW-DFC09$_x$ and vdW-DF2C09$_x$ schemes predict smaller interlayer distances in configurations $c_{12}$ and $c_{15}$ respectively. Similarly, LDA gives a slight decrease from 5.90 Å ($c_{12}$) to 5.84 Å ($c_{14}$) although both configurations are equivalent, whereas GGA-PBE shows a slight increase from 8.42 Å ($c_{12}$) to 8.51 Å ($c_{14}$), respectively. More importantly, apart from the vdW-DFC09$_x$ functional, all other schemes show that $d_0$ is consistently larger when the dimer forms vertically in configuration $c_{15}$ compared to when it forms horizontally in configuration $c_{12}$.

Taken together, these interlayer distances are large relative to the equilibrium interlayer distances in pristine graphene bilayer (see Table I). We ascribe the large interlayer distances to the decoupling of the bound bilayer graphene because of formation of the molecular hydrogen. The dimer formation breaks the symmetry of bilayer graphene structure. In the relaxed state, the large interlayer distances in configurations $c_{12}$, $c_{14}$, and $c_{15}$ imply that the two bound monolayers of graphene are no longer coupled, and are therefore structurally not equivalent to the coupled bilayer system in configuration $c_1$. This is due to weakened van der Waals interactions between layer A and B. The formation of the dimer in the interlayer region is analogous to hydrogen intercalation of bilayer graphene. By extension, we suggest the mechanism of hydrogen intercalation of graphite as a promising method of exfoliating graphene monolayers.

### 2. *Formation energy of hydrogenated bilayer graphene*

Competing low energy configurations of hydrogenated bilayer graphene are identified by investigating the formation energy per carbon atom. The formation energy was obtained using the expression[24]

$$E_f = [E_{H-b} - N_C \times E_G - N_H \times \frac{1}{2} E_{H_2}]/N_C, \qquad (1)$$

where $E_{H-b}$ is the energy of relaxed hydrogenated bilayer graphene, $E_G$ and $E_{H_2}$ are the total energy per atom of the graphite and hydrogen molecule ($H_2$). $N_C$ and $N_H$ denote the total number of carbon and hydrogen atoms in the $1 \times 1$ unit cell. Formation energies are presented for LDA, GGA and the four implementations of the non-local vdW corrections to compare their relative stabilities and to predict the competing low energy structures at 0 K.

Fig. 3 shows the formation energy per carbon atom in structurally unique configurations of hydrogenated bilayer graphene from six XC functionals. In the cases where more than one configuration presents the same formation energy, only one formation energy is presented. The LDA gives the lowest formation energies $E_f$ compared to GGA and vdW-DF. The high formation energies indicate that it is energetically more expensive to create these configurations. In the relaxed state of configuration $c_{10}$, the local structure shows that the H-adatom on the direct carbon of the interlayer region (i.e. hydrogen atom adsorbed on site $b'_{above}$) undergoes interlayer diffusion, and migrates to occupy another on top site. This further confirms the affinity of hydrogen to the on top site in graphene monolayers. However, the local structure in configuration $c_{10}$ is equivalent to that in configuration $c_2$ because the difference between their heats of formation is 0.002

eV (LDA), 0.0 eV (GGA) and 0.001 eV (vdW-DF). Hence the two configurations are energetically equivalent in their relaxed states.

The vdW-DF schemes yield the same formation energies in energetically equivalent structures. For instance, we obtain -0.13 eV (vdW-DF) and -0.23 eV (vdW-DF2) in configurations $c_{12}$ and $c_{14}$, and -0.13 eV (vdW-DF) and -0.22 eV (vdW-DF2) in configuration $c_{15}$. These energies change to -0.20 eV (vdW-DFC09$_x$) and -0.11 eV (vdW-DF2C09$_x$) in $c_{12}$ and $c_{14}$ respectively, and -0.21 eV (vdW-DFC09$_x$) and -0.11 eV (vdW-DF2C09$_x$) respectively in configuration $c_{15}$. Because the energy of formation of the vertical dimer in configuration $c_{15}$ is different from the energy required to form horizontal dimers in both configurations $c_{12}$ and $c_{14}$, we identify the formation of both dimer orientations as unique.

We identify six energetically favorable configurations at 0 K. These are configurations $c_1$, $c_2$, $c_7$, $c_8$, $c_{12}$ and $c_{15}$. Only configurations $c_1$, $c_2$, $c_7$ and $c_8$ retain the coupled bilayer structure in the relaxed state. Because configuration $c_8$ is known[39] to undergo a hydrogen-induced phase transformation from hexagonal to tetrahedral geometry, we suggest that the four low energy configurations are competing structures at 0 K. Our calculated formation energies for configuration $c_8$ from both LDA, GGA and vdW-DF functionals agree with the GGA and LDA calculations of Leenaerts *et al.*[39] Apart from configurations $c_1$ and $c_{12}$, the LDA gives comparatively lower formation energies than GGA and the vdW-corrected functionals. We observe that GGA and vdW-DF yield nearly the same formation energies for configurations $c_3$, $c_4$, $c_5$, $c_8$, $c_{10}$, $c_{13}$ and $c_{16}$. The formation energy differences $\Delta E_f$ between GGA and vdW-DF in configuration $c_1$ is slightly more than 0.05 eV, but less than 0.03 eV in configuration $c_4$, $c_5$ and $c_{10}$ (see Fig. 3). Our LDA calculation gives small positive formation energy in configuration $c_1$, whereas both vdW-DF and GGA yields a negative enthalpy of formation suggesting that configuration $c_1$ may form spontaneously. The low formation energy from vdW-DF in $c_1$ suggests that the binding force between the molecular hydrogen and the bilayer graphene arises from van der Waals interaction because the $H_2$ dimer is physisorbed above layer A (see Fig. 2(a)).

The hydrogen adatoms are all chemisorbed in the relaxed state, except in configurations $c_1$, $c_{12}$, $c_{14}$ and $c_{15}$, as shown in Table II. The local structures of competing low energy structures are shown in Fig. 4 for the relaxed states. These suggest that the properties of the hydrogenated bilayer graphene configurations are sensitive to the location of the carbon atom in the unit cell, and on the hydrogen adsorption site geometries. The top layers in configurations $c_2$ and $c_7$ are equivalent to the stable structure of monolayer graphene under the condition of 100 % H-coverage. The resulting graphane structure is known to be stable both theoretically[24] and experimentally.[15] In the theoretical study of Sofo *et al.*,[24] the GGA functional predicted short, and strong covalent bonds between hydrogen and carbon atoms.

Fig. 3 shows that the most stable configuration of hydrogen adatoms on the bilayer graphene (*i.e.* with the lowest formation energy) is obtained when sites $b_{above}$ $a'_{below}$ are fully saturated (Table II). The resulting local structure is equivalent to the bilayer analogue of graphane - a fully hydrogenated graphene monolayer. Table II shows the properties of coupled structures of pristine and hydrogenated bilayer graphene after relaxation. All the XC functionals give the same bond length ($l_{C\text{-}C}$ = 1.429 Å) and bond angle ($\theta$ = 120°) in the pristine bilayer. Similarly, hydrogen adsorption causes an increase in mean bond-length towards the value of 1.51Å expected in the diamond structure, while bond angles simultaneously decrease towards sp$^3$-hybridized angle of 109.7°. The inclusion of non-local vdW corrections show minimal deviations in the bond length and bond angle of configuration $c_8$ relative to values expected in graphane[24,39] while configurations $c_2$ and $c_7$ give slightly larger values (see Table III). Because the experimental value of the layer-layer separation in pristine bilayer is 3.35 Å[35] we conclude that LDA gives the most accurate bilayer separation, although in configurations $c_2$ and $c_7$, it overestimates it by 10.3 %. Within vdW-correction, the interlayer distance is both underestimated; 3.29 Å (vdW-DF2C09$_x$) and 3.27 Å (vdW-DFC09$x$), and overestimated; 3.51 Å (vdW-DF) and 3.59 Å (vdW-DF2) in the pristine bilayer. Both vdW-schemes and GGA overestimates the layer-layer distance of the bilayer by a maximum of 21.4 % and 41.3 % respectively.

Table III shows significantly reduced interlayer distance in configuration $c_8$ after structural relaxation. Configurations $c_2$ and $c_8$ exhibit the largest deviations in bond angles, $\theta$. Their low total energies, and heats of formation at 0 K after correcting for vdW interactions (see Fig. 3) suggest that their high relative stability could be ascribed to puckering- mechanism, in good agreement with Sofo *et al.*[24] Thus, although the adsorption of hydrogen atoms on a single sublattice of either plane A or plane B of the bilayer graphene structure does not result in any stable structure, hydrogenating both external faces, specifically at site $b_{above}a'_{below}$ (see Table II) gives rise to the most stable configuration. Our results confirms the recent observation[39] that adsorption of hydrogen on the both faces of bilayer graphene, at 50% coverage, causes the transformation of the structure to the tetrahedral geometry. In this H-mediated transformation, both the top and bottom layer carbon atoms come into sufficiently close proximity to allow interlayer chemical bonds to form between them. This is also accompanied by a change in the hybridization of the carbon bonds from sp$^2$ to sp$^3$ resulting in increased mean bond length from 1.42Å in pristine bilayer to 1.51Å expected in the diamond structure. The low formation energy observed in configuration $c_8$ suggests that the interlayer bond-formation mechanism favors the binding of hydrogen atoms to the two external faces of the bilayer in order to form the interlayer bond. As suggested by Leenaerts *et al.*,[39] the implication is that both sides of the bilayer graphene has to be exposed to hydrogen for the transformation to occur because graphene is hard to penetrate.[63,64]

In configurations $c_2$ and $c_7$, the bond lengths in the hydrogen-free bottom layer still retain their graphitic values of 1.42 Å. The difference between the H-adsorption sites in configurations $c_2$ and $c_7$ (see Fig. 4) results in nontrivial differences in the interlayer separation in the two configurations (as shown in Table III). All the exchange-correlation functionals consistently give wider interlayer separation in configuration

$c_7$ compared to configuration $c_2$. The physical justification for the wider interlayer in configuration $c_7$ is unclear, since the bottom layer in both structures are unhydrogenated. Nevertheless, it suffices to attribute the wide interlayer separation in configuration $c_7$ to the fact that the interlayer adsorption of the hydrogen atom directly on top of the bottom layer carbon gives rise to a higher local displacement of the top layer compared to configuration $c_2$. Since the interlayer hydrogen atom in configuration $c_2$ is not located on top of any atom of the bottom layer, the net interatomic repulsion is minimal, relative to configuration $c_7$.

Boukhvalov *et al.*[19] showed that adsorbing a single hydrogen atom on single layer graphene yields a positive activation energy, and thus its chemisorption energy is not favorable. In Fig. 3, configurations with high formation energies (*i.e.*, $E_f > 0.4$ eV) are considered metastable, and therefore are unstable at 0 K relative to configurations $c_2$, $c_7$, and $c_8$. It is relevant to note that configurations $c_4$ and $c_{10}$ are equivalent, with the hydrogen adsorption sites swapped. Because the formation energy of all the metastable configurations (see Fig. 3) are less than 1.00 eV relative to configurations $c_2$, $c_7$ and $c_8$, and consider that formation energies are determined with respect to graphite and molecular hydrogen, we conclude that it is distinctly possible to form these metastable configurations under finite temperature conditions if the temperature is high enough to overcome their formation barriers.[19]

In the case of single graphene layer, the effects of the hydrogen adatoms are balanced by the simultaneous adsorption of hydrogen atoms both above and below the layer. The observed instability in configuration $c_4$, $c_5$ and $c_{10}$ arises from the high chemisorption energy expected in a single H-adatom configuration. This is due to the absence of the hydrogen adatom on the opposite face of the top, and bottom, of monolayers. Otherwise, the presence of such configuration deviates from the 50% coverage hydrogen adatoms on bilayer graphene. Therefore, the absence of the single layer distortion-balancing effect must be responsible for the observed structural instability. The effect of this instability is clearly exhibited in the inconsistency in C-C bond lengths within the top and bottom layers of the metastable configurations.

In the electrostatic approximation, the top and bottom layers in the metastable configurations (*i.e,* $c_4$, $c_5$ and $c_{10}$) can be considered to carry charges $q_1$, $q_2$ and $q_3$ respectively, of the same magnitude. This implies that they carry equal charges on both layers, and are each separated by the corresponding interlayer distances. For the stable configurations, Table III shows that the interlayer separation varies significantly from the equilibrium value ($d_0$ = 3.35 Å), after relaxation. These variations arise from the competition between the Coulombic repulsion, the puckering effect of hydrogen, and van der Waals interactions between the polar layers. An effective polarity develops in the metastable configurations because the two unhydrogenated carbon atoms in the top and bottom layers are indirect. This implies that a large number of symmetry raising Jahn-Teller distortions are necessary to change the interplanar ordering from the Bernal (AB) stacking to the simple (AA) stacking sequence.

We therefore suggest that the high stability of competing low-energy, coupled hydrogenated bilayer, structures arise because the hydrogen adatoms are chemisorbed on indirect carbon atoms. Because the indirect carbon atoms are not positioned directly above each other along the $c$-axis, the effective repulsion between the carbon ion cores is minimized. The structural relaxation effects of the hydrogenation reduces the effective interlayer separation, such that $d \ll d_0$ as shown in Table III. The reduced interlayer separation therefore brings all the direct carbon atoms into sufficiently close contact, to allow the overlap of the atomic wave functions. This therefore creates strong C-C bonds due to the hydrogen-induced rehybridization of the atomic orbitals. Moreover, the interlayer separation in $c_8$ is equivalent to the C-C bond-length in the diamond structure. We therefore conclude that configuration $c_8$ represents a viable template for synthesizing nanodiamonds from graphene by hydrogenation. This is consistent with the observation of the formation of full $sp^3$-hybridized structure from hydrogen adsorption on bilayer graphene.[39]

### C. Electronic properties

Fig. 5(a)-(d) shows the band structures of pristine bilayer graphene from the four forms of the non-local vdW-functionals. The electronic states are labeled at high symmetry points of the Brillouin zone with reference to the Fermi level, in each case. These show a conical dispersion at the Γ-point, and a parabolic dispersion at the $K$-point, as expected. There are four $\pi$-bands which nearly meet at the $K$-point. The highest occupied molecular orbitals (HOMO) and lowest unoccupied molecular orbitals (LUMO) levels nearly coincide at Brillouin zone point $K$ giving rise to zero-band gap. Fig. 5 show that the four vdW-functionals give similar band structures for pristine bilayer graphene. Despite the similarities in the band structure, subtle differences are observed in the dependence of band energies on Brillouin zone direction ($E(k)$ dispersion) and energy eigenvalues at high symmetry points. The agreement of the vdW-interaction corrected band structures with LDA and GGA band structures is qualitative because although the $E(k)$ dispersion is correctly predicted, slight differences are observed in the band energies at high-symmetry points. Table IV shows the eigenvalues of the HOMO and LUMO levels in the pristine bilayer relative to the Fermi level calculated using the different functionals. After correcting for vdW-interactions, the maximum and minimum eigenvalues of the HOMO ($K_{1v}$) /LUMO ($K_{1c}$) level are 1.38 eV (vdW-DF2) and 1.21 eV (vdW-DFC09$_x$) in the pristine bilayer. The difference between the vdW-DF and vdW-DF2C09$_x$ eigenvalues for both HOMO and LUMO levels is 0.02 eV.

We have further investigated how the adsorbed hydrogen alters the electronic structures of bilayer graphene in all the structural configurations considered. For the pristine bilayer graphene, and for configurations $c_1$, $c_2$, $c_7$ and $c_8$, the band energies decrease significantly for all the functionals. Nevertheless, the HOMO/LUMO levels in configurations $c_2$ and $c_7$ are the same for all functionals, and coincide at point K in the Brillouin zone. These configurations show semimetallic

behavior except for configuration $c_8$, where there is an energy gap between the $\Gamma_{1v}$ and $\Gamma_{1c}$ levels. From Table IV, the calculated band gap (at Γ-point) in configuration $c_8$ is 2.80 eV (vdW-DF), 2.61 eV (vdW-DF2), 2.91 eV (vdW-DFC09$_x$), 2.90 eV (vdW-DF2C09$_x$), 2.89 eV (LDA) and 3.09 eV (GGA), respectively. It is noted in particular that the LDA and GGA energy gaps are in agreement with previous results.[39] We therefore conclude that use of the Cooper exchange functional (C09$_x$) in vdW-DF and vdW-DF2 has very minimal influence on the band gap of configuration $c_8$. The implication is that vdW interaction is not significant in configuration $c_8$ because of the formation of strong interlayer carbon bonds.

We also investigate the alignment of the hydrogen-induced energy bands in bilayer graphene. Because the electronic structures from LDA, GGA and the four schemes for vdW interaction correction are similar, we only show the vdW-DF band structures of selected hydrogenated configurations in Fig. 6. In configuration $c_1$, the physisorption does not alter the physical properties of the bilayer structure. However, in comparison with the pristine band structure, there are two extra bands due to hydrogen. These are denoted in Fig. 6(a) by $K_{3v}$ and $K_{3c}$. The extra bands are attributed H-H bonding in the $H_2$-dimer. The $K_{3v}$ band arises from the $\sigma$-bonding state between the two H $1s$-states, while $K_{3c}$ is an anti-bonding state. Nevertheless, the resulting structure is semimetalic. As seen in Sec.III(B), configurations $c_2$ and $c_7$ are similar - differing only in terms of their H-adsorption sites. In Table IV, the energy difference at $K_{1v}$ for configurations $c_2$ and $c_7$ is less than 0.01 eV. However configuration $c_7$ has a slightly lower Fermi energy compared to configuration $c_2$. Hence, we show the band structure for configuration $c_7$ in Fig. 6(b) for comparison with other configurations. In contrast with the pristine band structure, there are two linearly-dispersed bands instead of the four bands coinciding at point $K_1$. This also shows that the system is semimetalic. This same trend has also been seen experimentally by Nourbakhsh *et al.*[65] for oxygen adatoms on bilayer graphene. We find that by fully saturating the top layer in configuration $c_7$, the two $\pi$-bands at point $K$ reduce to one (see Fig. 6(b)). Fig. 6(c) shows that configuration $c_8$ gives rise to a wide band gap at point $K$. The relaxed geometry of configuration $c_8$ (see Fig. 4(c)) shows that the network structure is fully saturated. Because the interplanar C-C bond length (see Table III) is significantly reduced, strong $sp^3$ hybridized bonds form between neighboring C atoms and break the symmetry of the $\pi$-bands. The band structures in configurations $c_4$, $c_5$ and $c_{10}$ are the same, despite the differences in the positions of the adsorbed hydrogen atoms after relaxation. These are presented in Fig. 6(d), to show metallic transport at 0 K in these configurations because there are no HOMO and LUMO levels due to bands crossings at their Fermi levels.

The metastable configurations yield longer C-H bond lengths, and their band structures show metallic transport properties. We also investigate the influence of the C-H bond length on the electronic properties of configuration $c_8$. Fig. 7 shows the variations in band gap for the six XC functionals as a function of the C-H bond length. At the equilibrium C-H bond length (1.10 Å), all six functionals consistently give maximum band gaps. We find that the vdW-DF yields higher band gaps for stretched C-H bonds while compressed C-H bonds yield low band gaps. By contrast, the LDA and GGA give an opposing trend because the compression (or stretching) of C-H bonds give rise to higher (or lower) energy gaps. The GGA predicts larger band gaps in configuration $c_8$ for all C-H bond lengths. At the equilibrium C-H bond length vdW-DF yield the band gap. The vdW-DF2C09$_x$ functional predicts the lowest band gaps when the C-H bond lengths are stretched and, or compressed maximally. Both vdW-DF2 and vdW-DF2C09$_x$ give the same band gap (2.53 eV) when the bonds are fully stretched to 1.20 Å, but show a significant difference of 0.15 eV for compressed bonds.

## IV. CONCLUSIONS

This paper predicts, and characterizes the possible structural configurations for the adsorption of hydrogen atoms on bilayer graphene. Using different exchange-correlation functionals, the relative stabilities and electronic properties of the hydrogen-adsorbed bilayer graphene are explored at 0 K. We find that the different forms of the vdW-interaction corrections perform best in relaxed configurations where the $H_2$ dimer is physisorbed, and the graphene bilayers are decoupled. On the other hand, the LDA performs best in configurations where the bilayer graphene is coupled in the relaxed state, and the hydrogen atoms are chemisorbed. Our analyses of the formation energies show that six of the configurations can form spontaneously. Because of the low, albeit positive, heats of formation in the metastable configurations, we suggest that their formation can be achievable by activation. The spontaneous formation of the lowest energy configurations is strongly dependent on the arrangement of the adsorbed hydrogen atoms. It is noted that apart from configuration $c_1$, this spontaneous formation only occurs when the top layer of carbon atoms is fully saturated, leaving the bottom layer completely unhydrogenated, or when both top and bottom layers are partially hydrogenated. The partial hydrogenation of both the top and bottom layers is found to result in a non-reversible transformation of the graphenic hexagonal structure to local diamond, tetrahedral, structure. This H-induced local reconstruction results in shortened C-H bonds and a considerable buckling of the tetrahedral structure. Relatively longer C-H bonds are obtained in configurations that display non-spontaneous formation, and their local structures are only slightly buckled.

We conclude that hydrogen atoms adsorbed on the top and bottom faces within the interlayer region causes considerable interlayer repulsion, which leads to increased interlayer distances (see Table III). This suggests hydrogen intercalation as a means of exfoliating graphene. The relatively more stable competing configurations exhibit either semi-metallic or insulating properties, whereas all the unstable configurations are metallic. We find that configuration $c_8$ results in an insulator, displaying a wide band gap. For this structure, the GGA yields the largest band gap. It is therefore concluded that no single exchange-correlation functional is able to describe the energetics, stability and local structure properties of all the

configurations consistently.

## ACKNOWLEDGMENTS

R.E.M. is grateful to the National Research Foundation (NRF) and the University of Pretoria for financial support. A.M.U. acknowledges financial support from the University of Pretoria under E2020 Project No. 5. N.C. thanks the University of Pretoria and National Institute of Theoretical Physics for financial support.

* aniekan.ukpong@up.ac.za


[1] K. S. Novoselov, A. K. Geim, S. V. Morozov, D. Jiang, Y. Zhang, S. V. Dubonos, I. V. Grigorieva, and A. A. Firsov, Science **306**, 666 (2004).
[2] A. K. Geim and K. S. Novoselov, Nature Mater. **6**, 183 (2007).
[3] P. R. Wallace, Phys. Rev. **71**, 622 (1947).
[4] K. S. Novoselov, A. K. Geim, S. V. Morozov, D. Jiang, Y. Zhang, M. I. Katsnelson, S. V. Dubonos, I. V. Grigorieva, and A. A. Firsov, Nature (London) **438**, 197 (2005).
[5] Y. Zhang, Y. W. Tan, H. L. Stormer, and P. Kim, Nature (London) **438**, 201 (2005).
[6] A. H. Castro, F. Guinea, N. M. R. Peres, K. S. Novoselov, and A. K. Geim, Rev. Mod. Phys. **81**, 109 (2009).
[7] F. Schedin, A. K. Geim, S. V. Morozov, E. W. Hill, P. Blake, M. I. Katsnelson, and K. S. Novoselov, Nature Mater. **6**, 652 (2007).
[8] M. Terrones, B. R. Botello-Mendez, J. Campos-Delgado, F. Lopez-Urias, Y. I. Vega-Cantu, F. J Rodriguez-Macias, A. L. Elias, E. Munoz-Sandoval, A. G. Cano-Marquez, J. C. Chalier, and H. Terrones, Nano Today **5**, 351 (2010).
[9] J. A. Yan, L. Xian, and M. Y. Chou, Phys. Rev. Lett. **103**, 086802 (2009).
[10] X. S. Wu, M. Sprinkle, X. B. Li, F. Ming, C. Berger, and W. A. de Heer, Phys. Rev. Lett. **101**, 026801 (2008).
[11] I. Jung, D. A. Dikin, R. D. Piner, and R. S. Ruoff, Nano Lett. **8**, 4283 (2008).
[12] Z. Luo, P. M. Vora, E. J. Mele, A. T . C. Johnson, and J. M. Kikkawa, Appl. Phys. Lett. **94**, 111909 (2009).
[13] R. Balog, B. Jorgensen, L. Nilsson, M. Andersen, E. Rienks, M. Bianchi, M. Fanetti, E. Laegsgaard, A. Baraldi, S. Lizzit, Z. Sljivancanin, F. Besenbacher, B. Hammer, T. G. Pedersen, P. Hofmann, and L. Hornekaer. Nature Mater. **9**, 315 (2010).
[14] A. Savchenko, Science **323**, 589 (2009).
[15] D. C. Elias, R. R. Nair, T. M. G. Mohiuddin, S. V. Morozov, P. Blake, M. P. Halsall. A. C. Ferrari, D. W Boukhvalov, M. I. Katsnelson, A. K. Geim, and K. S. Novoselov, Science. **323**, 610 (2009).
[16] Y. H. Lu, W. Chen, Y. P. Feng, and P. M. He, J. Phys. Chem. B **113**, 2 (2009).
[17] I. Zanella, S. Guerini, S. B. Fagan, J. MendesFilho, and A. G. SouzaFilho, Phys. Rev. B **77**, 073404 (2008).
[18] R. M. Ribeiro, N. M. R. Peres, J. Coutinho, and P. R. Briddon, Phys. Rev. B **78**, 075442 (2008).
[19] D. W. Boukhvalov, M. I. Katsnelson, and A. I. Lichtenstein, Phys. Rev. B **77**, 035427 (2008).
[20] S. Lebegue, M. Klintenberg, O. Eriksson, and M. I. Katsnelson, Phys. Rev. B **79**, 245117 (2009).
[21] E. J. Duplock, M. Scheffler, and P. J. D. Lindan, Phys. Rev. Lett. **92**, 225502 (2004).
[22] D. W. Boukhvalov and M. I. Katsnelson, Phys. Rev. B **78**, 085413 (2008).
[23] N. Z. Lu, Z. Y. Li, and J. L. Yang, J. Phys. Chem. C **113**, 16741 (2009).
[24] J. O. Sofo, A. S. Chaudhari, and G. D. Barber, Phys. Rev. B **75**, 153401 (2007).
[25] L. Sun, Q. X. Li, H. Ren, H. B. Su, Q. W. Shi, and J. L. Yang, J. Chem. Phys **129**, 074074 (2008).
[26] Y. W. Son, M. L. Cohen, and S. G. Louie, Phys. Rev. Lett **97**, 216803 (2006).
[27] M. Y. Han, B. Ozyilmaz, Y. Zhang, and P. Kim, Phys. Rev. Lett **98**, 206805 (2007).
[28] F. Ding, Phys. Rev. B **72**, 245409 (2005).
[29] G. D. Lee, C. Z. Wang, E. Yoon, N. M. Hwang, D. Y. Kim, and K. M. Ho, Phys. Rev. Lett. **95**, 205501 (2005).
[30] M. T. Lusk and L. D. Carr, Phys. Rev. Lett. **100**, 175503 (2008).
[31] S. C Pradhan and J. K. Phadikar, Phys. Lett. A **373**, 1062 (2009).
[32] P. Lu, Z. Zhang, and W. Guo, Phys. Lett. **373**, 3354 (2009).
[33] W. Choi, I. Lahiri, R. Seelaboyina, and Y. S. Kang, Crit. Rev. Solid State and Mater Sci. **35**, 52 (2010).
[34] H. Min and A. H. MacDonald, Phys. Rev. B **77**, 155416 (2008).
[35] T. Ohta, A. Bostwick, T. Seyller, K. Horn, and E. Rotenberg, Science **313**, 951 (2006).
[36] Z. Q. Luo, T. Yu, K. J. Kim, Z. H. Ni, Y. M. You, S. H. Lim, Z. X. Shen, S. Z. Wang, and J. Y. Lin, ACSNANO **3**, 1781 (2009).
[37] K. S. Subrahmanyam, P. Kumar, U. Maitra, A. Govindaraj, K. P. Hembram, U. V. Waghmare, and C. N. R. Rao, Proc. Nat. Acad. Sci. (USA) **108**, 2677 (2011).
[38] M. Jaiswal, C. H. Lim, Q. Bao, C. T. Toh, K. P. LOh, and B. Ozyilmaz, ACSNANO **5**, 888 (2011).
[39] O. Leenaerts, B. Partoens, and F.M. Peeters, Phys. Rev. B **80**, 245422 (2009).
[40] S. M. Choi, S. H. Jhi, and Y. W. Son, Nano. Lett. **10**, 3486 (2010).
[41] P. L. de Andres, R. Ramirez, and J. A. Verges, Phys. Rev. B **77**, 045403 (2008).
[42] P. Giannozzi, S. Baroni, N. Bonini, M. Calandra, R. Car, C. Cavazzoni, D. Ceresoli, G. L. Chiarotti, M. Cococcioni, I. Dabo, A. Dal Corso, S. Fabris, G. Gougoussis, A. Kokalj, M. Lazzeri, L. Martin-Samos, N. Marzari, F. Mauri, R. Mazzarello, S. Paolini, A. Pasquarello, L. Paulatto, C. Sbraccia, S. Scandolo, G. Sclauzero, A. P. Seitsonen, A. Smogunov, P. Umari, and R. M. Wentzcovitch, J. Phys. Condens. Matter **21**, 395502 (2009).
[43] J. P. Perdew and A. Zunger, Phys. Rev. B **23**, 5048 (1981).
[44] J. P. Perdew, K. Burke, and M. Ernzerhof, Phys. Rev. Lett. **77**, 3865 (1996).
[45] G. Roman-Perez and J. M. Soler, Phys. Rev. Lett. **103**, 096102 (2009).
[46] M. Dion, H. Rydberg, E. Schroder, D. C. Langreth, and B. I. Lundqvist, Phys. Rev. Lett. **92**, 246401 (2004).
[47] K. Lee, E. D. Murray, L. Kong, B. I. Lundqvist, and D. C. Langreth, Phys. Rev. B **82**, 081101 (2010).
[48] E. D. Murray, K. Lee, and D. C. Langreth, J. Chem. Theory Comput. **5**, 2754 (2009).
[49] J. P. Perdew and Y. Wang, Phys. Rev. B **33**, 8800 (1986).
[50] V. R. Cooper, Phys. Rev. B **81**, 161104 (2010).
[51] P. E. Blochl, Phys. Rev. B **50**, 17953 (1994).

[52] H. J. Monkhorst and J. D. Pack, Phys. Rev. B **13**, 5188 (1976).
[53] M. Methfessel, and A. T. Paxton, Phys. Rev. B **40**, 3616 (1989).
[54] I. Hamada and M. Otani, Phys. Rev. B **82**, 153412 (2010).
[55] H. Rydberg, M. Dion, N. Jacobson, E. Schroder, P. Hyldgaard, S. I. Simak, D. C. Langreth, and B. I. Lundqvist, Phys. Rev. Lett. **91**, 126402 (2003).
[56] This value of interlayer distance is obtained as half of the geometrical parameter from Table I of Ref. 55.
[57] S. D. Chakarova-Kack, E. Schroder, B. I. Lundqvist, and D. C. Langreth, Phys. Rev. Lett. **96**, 146107 (2006).
[58] Y. Baskin and L. Mayer, Phys. Rev **100**, 544 (1955).
[59] R. Zacharia, H. Ulbricht, and T. Hertel, Phys. Rev. B **69**, 155406 (2004).
[60] L. X. Benedict, N. G. Chopra, M. L. Cohen, A. Zettl, S. G. Louie, and V. Crespie, Chem. Phys. Lett. **286**, 490 (1998).
[61] See Table SIV in the supplementary material of Ref. 54. Available online at: http://link.aps.org/supplemental/10.1103/PhysRevB.82.153412
[62] Note that this GGA-PBE data is obtained from dispersion-corrected atom-centred potential (DCAP) calculations.
[63] J. S. Bunch, S. S. Verbridge, J. S. Alden, A. M. van der Zande, J. M. Parpia, H.G. Craighead, and P. L. McEuen, Nano Lett. **8**, 2458 (2008).
[64] O. Leenaerts, B. Partoens, and F. M. Peeters, Appl. Phys. Lett. **93**, 193107 (2008).
[65] A. Nourbakhsh, M. Cantoro, A. V. Klekachev, G. Pourtois, T. Vosch, J. Hofkens. M. H. van der Veen. M. M. Heyns. S. DeGendt, and B. F. Sels, J. Phys. Chem. C **115**, 16619 (2011).

TABLE I. Properties of graphite and pristine bilayer graphene calculated using different exchange-correlation functionals to show the equilibrium lattice constants $a_0$, interlayer distances $d_0$ and the interlayer binding energies $E_B$. Results of our calculations are marked with an asterisk (*). The vdW-DF exfoliation energy of graphite is also shown (in parenthesis).

| | Graphite | | | Bilayer | | |
|---|---|---|---|---|---|---|
| Functionals | $a_0$ (Å) | $d_0$ (Å) | $E_B$ (meV) | $a_0$ (Å) | $d_0$ (Å) | $E_B$ (meV) |
| LDA* | 2.45 | 3.25 | 27.70 | 2.45 | 3.33 | 17.30 |
| LDA | 2.44[a] | 3.32[a] | (-26.00)[a] | | 3.30[h] | 13.98[h] |
| GGA* | 2.47 | 4.10 | 3.00 | 2.46 | 4.10 | 3.00 |
| GGA | 2.46[a] | 4.50[a] | (-2.00)[a] | | 3.32[i] | 27.00[i] |
| vdW-DF* | 2.48 | 3.57 | 55.00 | 2.47 | 3.51 | 22.70 |
| vdW-DF | | | (-52.00)[a] | | 3.58[h] | 25.43[h] |
| vdW-DF | 2.47[b] | 3.76[c] | 24.00[b] | | | |
| vdW-DF | | 3.60[d] | 45.50[d] | | | |
| vdW-DF2* | 2.47 | 3.49 | 66.00 | 2.47 | 3.49 | 29.00 |
| vdW-DF2 | | | (-53.00)[a] | | 3.48[h] | 25.84[h] |
| vdW-DF C09$_x$* | 2.48 | 3.25 | 91.00 | 2.48 | 3.27 | 38.90 |
| vdW-DF C09$_x$ | | | (-73.00)[a] | | 3.23[h] | 35.63[h] |
| vdW-DF2 C09$_x$* | 2.47 | 3.29 | 59.60 | 2.48 | 3.29 | 28.60 |
| vdW-DF2 C09$_x$ | | | (-54.00)[a] | | 3.28[h] | 25.86[h] |
| Experimental | 2.46[e] | 3.35[e] | 52±5[f], 35±10[g] | 2.46[j] | 3.40[j] | |

[a]Reference[54]
[b]Reference[55]
[c]Reference[56]
[d]Reference[57]
[e]Reference[58]
[f]Reference[59]
[g]Reference[60]
[h]Reference[61]
[i]Reference[62]
[j]Reference[35]

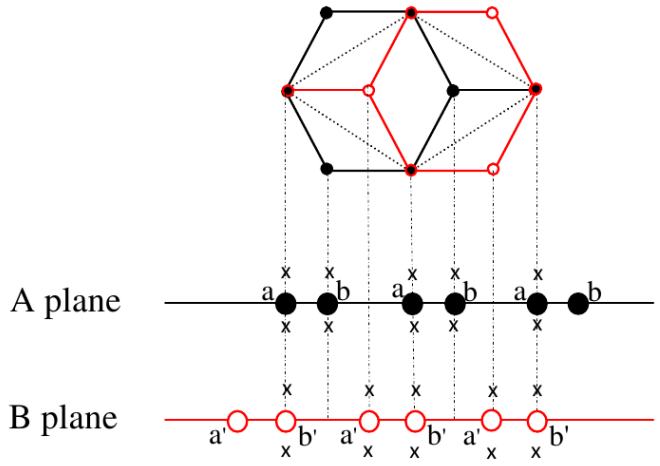


FIG. 1. Hydrogen adsorption sites (marked x) in the unrelaxed state of the bilayer graphene unit cell. The carbon atoms denoted by $a$ and $b'$ are the direct carbon atoms, while atoms $b$ and $a'$ are the indirect carbon atoms.

TABLE II. Configurations of hydrogenated bilayer at 50 % coverage and the corresponding hydrogen adsorption site geometries in the unrelaxed and relaxed states showing the changes in the local structure after structure optimization.

| Configurations | Geometry of the H adatom site | | Structural transformations |
|---|---|---|---|
| | Unrelaxed state | Relaxed state | |
| $c_1$ | $a_{above}b_{above}$ | $a_{above}a_{above}$ | Formation of horizontal $H_2$ dimer |
| $c_2$ | $a_{above}b_{below}$ | $a_{above}b_{below}$ | None ($c_2$ is symmetrical to $c_{10}$ by translation) |
| $c_3$ | $a_{above}a'_{above}$ | $a_{above}a'_{above}$ | None |
| $c_4$ | $a_{above}b'_{above}$ | $a_{above}b'_{above}$ | None |
| $c_5$ | $a_{above}b'_{below}$ | $a_{above}b'_{below}$ | None |
| $c_6$ | $a_{above}a'_{below}$ | $a_{above}a'_{below}$ | None |
| $c_7$ | $b_{above}a_{below}$ | $b_{above}a_{below}$ | None |
| $c_8$ | $b_{above}a'_{below}$ | $b_{above}a'_{below}$ | Formation of diamond-like structure |
| $c_9$ | $b_{above}a'_{above}$ | $b_{above}a'_{above}$ | None |
| $c_{10}$ | $b_{above}b'_{above}$ | $a_{below}b_{above}$ | One hydrogen site is swapped ($c_{10}$ relaxes to $c_2$) |
| $c_{11}$ | $b_{above}b'_{below}$ | $b_{above}b'_{below}$ | None |
| $c_{12}$ | $a'_{above}b_{below}$ | $a'_{above}a'_{above}$ | Formation of horizontal $H_2$ dimer ($c_{12}$ relaxes to $c_{14}$) |
| $c_{13}$ | $a'_{above}a_{below}$ | $a'_{above}a_{below}$ | None |
| $c_{14}$ | $a'_{above}b'_{above}$ | $a'_{above}a'_{above}$ | Formation of horizontal $H_2$ dimer ($c_{14}$ relaxes to $c_{12}$) |
| $c_{15}$ | $b'_{above}a_{below}$ | $b'_{above}a_{below}$ | Formation of vertical $H_2$ dimer |
| $c_{16}$ | $b'_{above}b_{below}$ | $b'_{above}b_{below}$ | None |

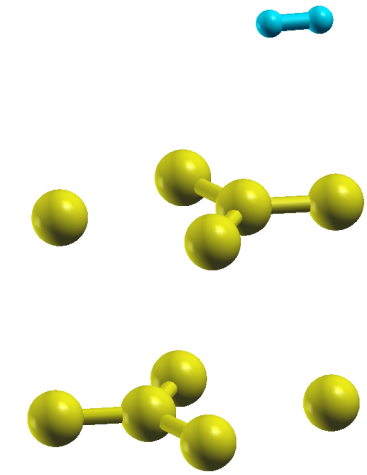

(a)

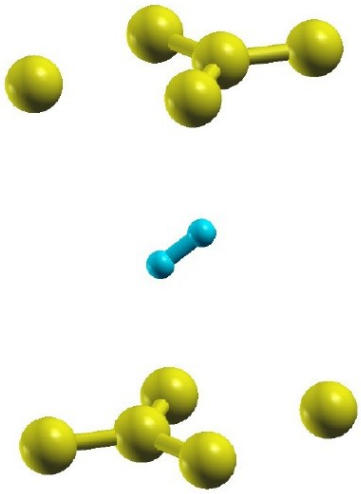

(b)

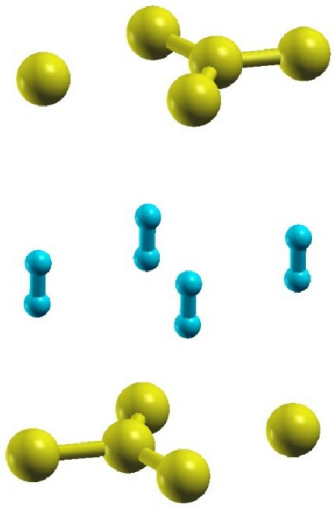

(c)

FIG. 2. Relaxed configurations showing the formation of the $H_2$ dimer: (a) above bilayer graphene in configuration $c_1$, and within the interlayer region of the decoupled bilayer graphene showing (b) horizontal intercalation in configurations $c_{12}$ and $c_{14}$, and vertical intercalation in configuration $c_{15}$.

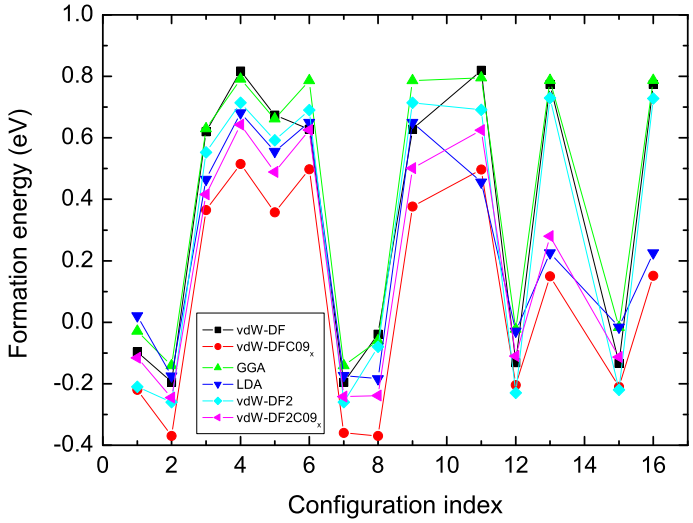


FIG. 3. Formation energies of unique configurations of hydrogenated bilayer graphene obtained using the LDA, GGA and the four different applications of the non-local van der Waals correlation functional.

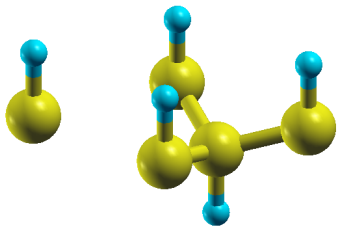

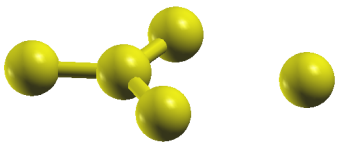

(a)

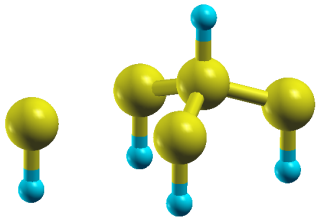

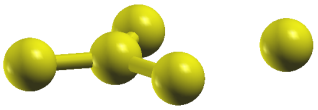

(b)

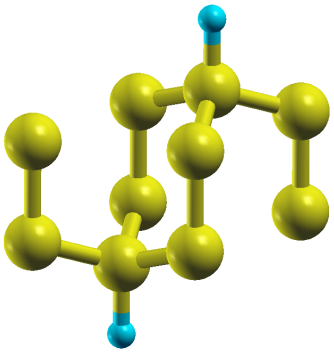

(c)

FIG. 4. Relaxed geometries of competing low-energy structures of coupled bilayer graphene at 50% hydrogen coverage showing configurations: (a) $c_2$, (b) $c_7$, and (c) $c_8$.

TABLE III. The calculated properties of selected competing structural configurations: the distances between two bonded carbon atoms $l_{\text{C-C}}$ (in Å), the bond angles $\theta_{\text{C-C-C}}$ (in degrees) and the interlayer distances $d_0$ (in Å). The $l_{\text{C-C}}$ bond lengths are quoted to three decimal places to demonstrated the similarity of the results for the six exchange correlation functionals.

| | | Top (bottom) layers of structural configurations | | | | | | | |
|---|---|---|---|---|---|---|---|---|---|
| | | Pristine | | 2 | | 7 | | 8 | |
| Parameters | Functionals | T | B | T | B | T | B | T | B |
| $l_{\text{C-C}}$ | vdW-DF | 1.429 | (1.429) | 1.498 | (1.429) | 1.498 | (1.429) | 1.504 | (1.504) |
| | vdW-DF2 | 1.429 | (1.429) | 1.501 | (1.429) | 1.505 | (1.429) | 1.514 | (1.514) |
| | vdW-DF C09$_x$ | 1.429 | (1.429) | 1.503 | (1.429) | 1.503 | (1.429) | 1.513 | (1.513) |
| | vdW-DF2 C09$_x$ | 1.429 | (1.429) | 1.504 | (1.429) | 1.504 | (1.429) | 1.512 | (1.512) |
| | LDA | 1.420 | (1.420) | 1.500 | (1.421) | 1.500 | (1.421) | 1.509 | (1.509) |
| | GGA | 1.429 | (1.429) | 1.504 | (1.430) | 1.504 | (1.430) | 1.512 | (1.512) |
| $\theta_{\text{C-C-C}}$ | vdW-DF | 120.0 | (120.0) | 110.4 | (120.0) | 110.4 | (120.0) | 109.8 | (109.8) |
| | vdW-DF2 | 120.0 | (120.0) | 110.9 | (120.0) | 110.7 | (120.0) | 109.8 | (109.8) |
| | vdW-DF C09$_x$ | 120.0 | (120.0) | 110.9 | (120.0) | 110.9 | (120.0) | 109.9 | (109.9) |
| | vdW-DF2 C09$_x$ | 120.0 | (120.0) | 110.8 | (120.0) | 110.8 | (120.0) | 110.0 | (110.0) |
| | LDA | 120.0 | (120.0) | 111.2 | (120.0) | 111.2 | (120.0) | 110.3 | (110.3) |
| | GGA | 120.0 | (120.0) | 110.8 | (120.0) | 110.8 | (120.0) | 109.9 | (109.9) |
| $d_0$ | vdW-DF | 3.51 | | 4.06 | | 4.14 | | 1.57 | |
| | vdW-DF2 | 3.59 | | 3.96 | | 4.05 | | 1.58 | |
| | vdW-DF C09$_x$ | 3.27 | | 3.69 | | 3.87 | | 1.58 | |
| | vdW-DF2 C09$_x$ | 3.29 | | 3.86 | | 3.87 | | 1.56 | |
| | LDA | 3.33 | | 3.69 | | 3.88 | | 1.55 | |
| | GGA | 4.10 | | 4.73 | | 4.85 | | 1.56 | |

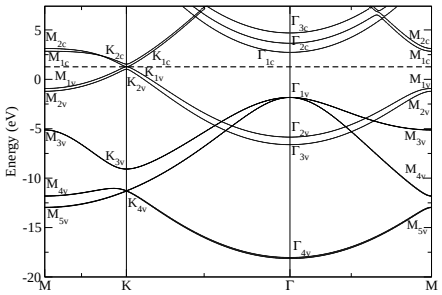


(a)

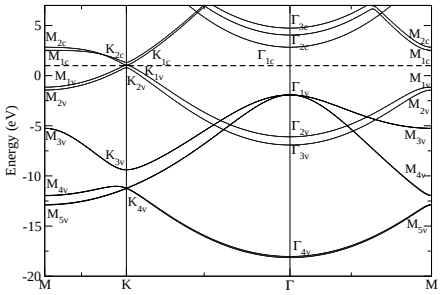


(b)

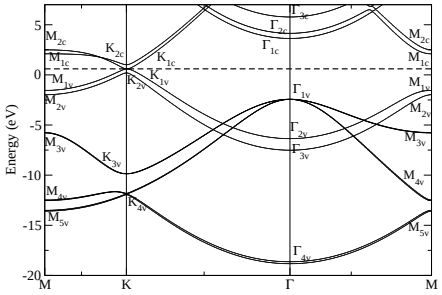


(c)

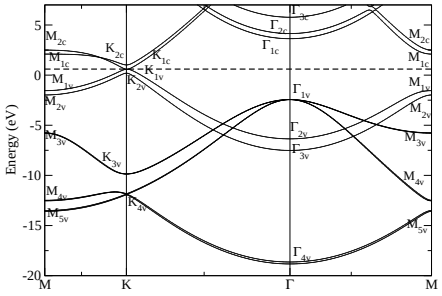


(d)

FIG. 5. Electronic band structure of pristine bilayer graphene calculated from four vdw-DF functionals: vdW-DF (a), vdW-DF2 (b), vdW-DFC09$_x$ (c), and vdW-DF2C09$_x$(d). The Fermi level is marked by the dotted line.

TABLE IV. The HOMO and LUMO eigenvalues (in meV) of structural configurations at high-symmetry points.

| Electronic states | Configurations | k-point | vdW-DF | vdW-DF2 | vdW-DF C09$_x$ | vdW-DF2 C09$_x$ | LDA | GGA |
|---|---|---|---|---|---|---|---|---|
| | pristine | $K_{1v}$ | 1.26 | 1.38 | 1.21 | 1.28 | 1.04 | 1.32 |
| | 1 | $K_{1v}$ | 1.10 | 1.09 | 1.07 | 1.09 | 0.89 | 1.19 |
| | 2 | $K_{1v}$ | 0.67 | 0.75 | 0.85 | 0.86 | 0.69 | 0.95 |
| | 7 | $K_{1v}$ | 0.65 | 0.71 | 0.83 | 0.84 | 0.71 | 0.95 |
| HOMO level | 8 | $\Gamma_{1v}$ | 0.78 | 0.59 | 0.61 | 0.69 | 0.91 | 1.10 |
| | pristine | $K_{1c}$ | 1.26 | 1.38 | 1.21 | 1.28 | 1.04 | 1.32 |
| | 1 | $K_{1c}$ | 1.10 | 1.09 | 1.07 | 1.09 | 0.89 | 1.19 |
| | 2 | $K_{1c}$ | 0.67 | 0.75 | 0.85 | 0.86 | 0.69 | 0.95 |
| | 7 | $K_{1c}$ | 0.65 | 0.71 | 0.83 | 0.84 | 0.71 | 0.95 |
| LUMO level | 8 | $\Gamma_{1c}$ | 3.58 | 3.20 | 3.52 | 3.59 | 3.78 | 4.19 |

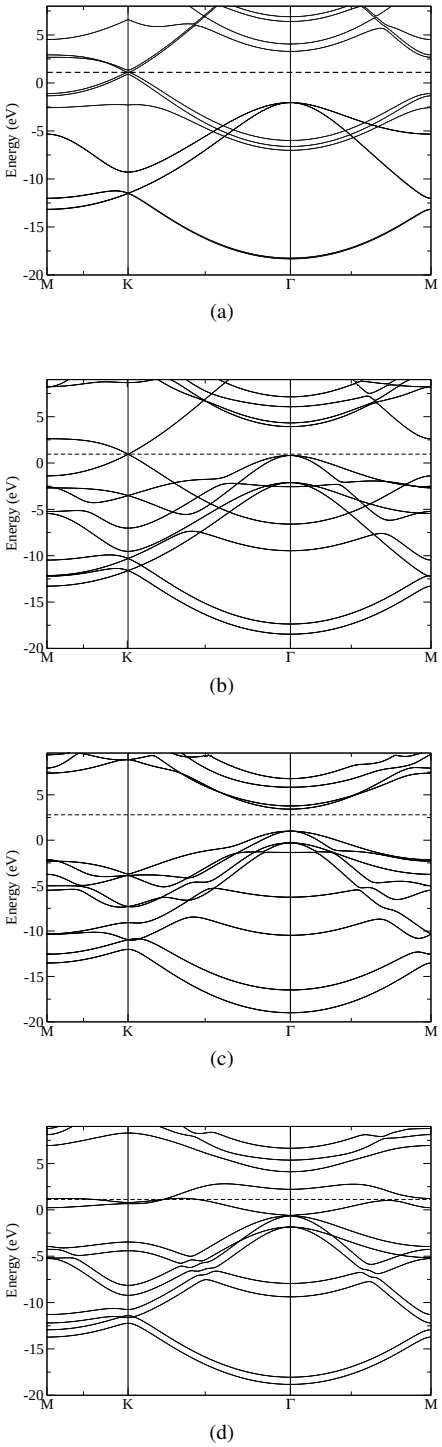


FIG. 6. The vdW-DF electronic band structure of $c_1$ (a); $c_7$ (b); $c_8$ (c); and $c_{10}$ (d). The Fermi level is marked by the dotted line

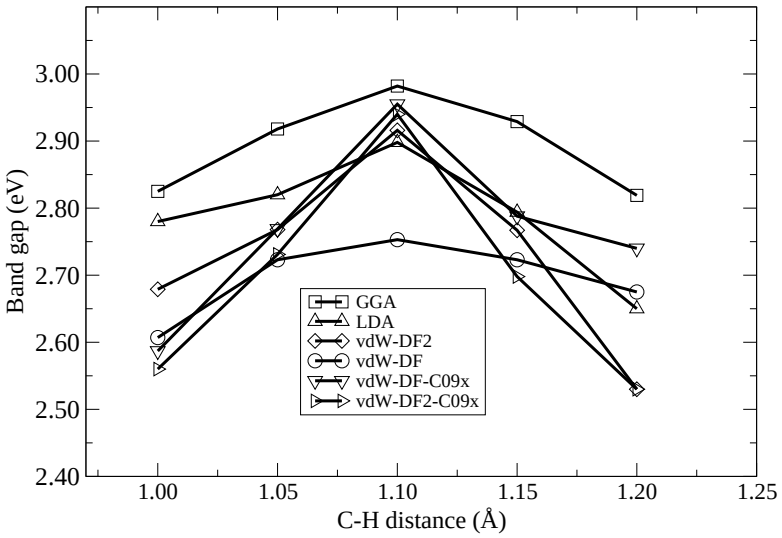


FIG. 7. Band gap of configuration $c_8$ as a function of C-H bond lengths predicted from six exchange-correlation functionals.